ESC European Society of Cardiology

Cardiovascular Research (2019) **115**, 1659–1671
doi:10.1093/cvr/cvz039

In vivo ratiometric optical mapping enables high-resolution cardiac electrophysiology in pig models

Peter Lee[1†], Jorge G. Quintanilla[2,3,4†], José M. Alfonso-Almazán[2], Carlos Galán-Arriola[2], Ping Yan[5], Javier Sánchez-González[6], Nicasio Pérez-Castellano[3,4], Julián Pérez-Villacastín[3,4,7], Borja Ibañez[2,3,8], Leslie M. Loew[5]*, and David Filgueiras-Rama[2,3,4]*

[1]Essel Research and Development Inc., Toronto, 337 Sheppard Ave East, Toronto, Ontario M2N 3B3, Canada; [2]Spanish National Cardiovascular Research Center, Carlos III (CNIC), Myocardial Pathophysiology Area, Melchor Fernández Almagro, 3, 28029 Madrid, Spain; [3]Centro de Investigación Biomédica en Red de Enfermedades Cardiovasculares (CIBERCV), Av. Monforte de Lemos 3-5, 28029, Madrid, Spain; [4]Arrhythmia Unit, Cardiovascular Institute, Instituto de Investigación Sanitaria del Hospital Clínico San Carlos (IdISSC), Prof. Martín Lagos s/n, 28040, Madrid, Spain; [5]Richard D. Berlin Center for Cell Analysis and Modeling, University of Connecticut School of Medicine, 263 Farmington Avenue, Farmington, CT 06030-6406, USA; [6]Philips Healthcare Iberia, María de Portugal 1, 28050, Madrid, Spain; [7]Fundación Interhospitalaria para la Investigación Cardiovascular (FIC), Paseo de San Francisco de Sales 3, 28003, Madrid, Spain; and [8]IIS-University Hospital Fundación Jiménez Díaz, Department of Cardiology, Av. Reyes Católicos 2, 28040, Madrid, Spain

Received 21 May 2018; revised 31 January 2019; editorial decision 4 February 2019; accepted 6 February 2019; online publish-ahead-of-print 7 February 2019

Time for primary review: 18 days

Aims Cardiac optical mapping is the gold standard for measuring complex electrophysiology in *ex vivo* heart preparations. However, new methods for optical mapping *in vivo* have been elusive. We aimed at developing and validating an experimental method for performing *in vivo* cardiac optical mapping in pig models.

Methods and results First, we characterized *ex vivo* the excitation-ratiometric properties during pacing and ventricular fibrillation (VF) of two near-infrared voltage-sensitive dyes (di-4-ANBDQBS/di-4-ANEQ(F)PTEA) optimized for imaging blood-perfused tissue ($n = 7$). Then, optical-fibre recordings in Langendorff-perfused hearts demonstrated that ratiometry permits the recording of optical action potentials (APs) with minimal motion artefacts during contraction ($n = 7$). Ratiometric optical mapping *ex vivo* also showed that optical AP duration (APD) and conduction velocity (CV) measurements can be accurately obtained to test drug effects. Secondly, we developed a percutaneous dye-loading protocol *in vivo* to perform high-resolution ratiometric optical mapping of VF dynamics (motion minimal) using a high-speed camera system positioned above the epicardial surface of the exposed heart ($n = 11$). During pacing (motion substantial) we recorded ratiometric optical signals and activation via a 2D fibre array in contact with the epicardial surface ($n = 7$). Optical APs *in vivo* under general anaesthesia showed significantly faster CV [120 (63–138) cm/s vs. 51 (41–64) cm/s; $P = 0.032$] and a statistical trend to longer APD_{90} [242 (217–254) ms vs. 192 (182–233) ms; $P = 0.095$] compared with *ex vivo* measurements in the contracting heart. The average rate of signal-to-noise ratio (SNR) decay of di-4-ANEQ(F)PTEA *in vivo* was $0.0671 \pm 0.0090\ min^{-1}$. However, reloading with di-4-ANEQ(F)PTEA fully recovered the initial SNR. Finally, toxicity studies ($n = 12$) showed that coronary dye injection did not generate systemic nor cardiac damage, although di-4-ANBDQBS injection induced transient hypotension, which was not observed with di-4-ANEQ(F)PTEA.

Conclusions *In vivo* optical mapping using voltage ratiometry of near-infrared dyes enables high-resolution cardiac electrophysiology in translational pig models.

Keywords *In vivo* imaging • Optical mapping • Voltage-sensitive dyes • Cardiac fibrillation • Cardiotoxicity

* Corresponding authors. Tel: (860) 679 3568; fax: (860) 679 1039, E-mail: les@uchc.edu (L.M.L.); Tel:+34 914531200; fax: +34 91 4531265, E-mail: david.filgueiras@cnic.es (D.F.-R.)

† Joint first authors. These authors contributed equally to this work.

1. Introduction

For decades, the goal of cardiac electrophysiology procedures has been to obtain accurate information regarding cardiac electrical activation during both normal sinus rhythm and various types of arrhythmias.[1–4] Current clinical approaches map cardiac electrical activity from the endocardial or epicardial surface of the heart using electrical signals acquired from bipolar or unipolar electrograms.[3–5] This electrical data can then be integrated with 3D anatomical surfaces to facilitate localization of specific activation patterns.[6,7] However, neither bipolar nor unipolar recordings enable the measurement of action potentials (APs) from the myocardium. Bipolar signals can estimate activation times, while unipolar signals can estimate both activation and repolarization times.[8,9] Furthermore, these estimations become more difficult in regions with poor signal quality that are often associated with scarred tissue.[10,11]

To date, the best method of probing cellular electrophysiology in the whole heart is optical mapping.[12] Optical mapping uses high-speed cameras or optical sensors to record fluorescence changes on the epicardial or endocardial surface of isolated Langendorff-perfused hearts, following injection of excitation-contraction uncouplers and voltage- or calcium-sensitive dyes.[13] This approach measures APs or calcium transients at high spatiotemporal resolution and has led to important milestones in the understanding of cardiac electrophysiology and the mechanisms of complex arrhythmias.[2,14] Despite the immensely fruitful impact of such *ex vivo* optical mapping studies, maintaining the native connections to the nervous and endocrine systems, may be critical to the study of certain arrhythmias.[15] However, to make progress in this area, two key issues need to be addressed: (i) the use of excitation-contraction uncouplers to minimize motion artefacts in fluorescence signals is not a viable option *in vivo*; and (ii) voltage-sensitive dyes might be toxic to vital organs, which has not been thoroughly investigated *in vivo*.

Here, we aimed at developing and validating an experimental method for performing *in vivo* optical mapping in a pig animal model with high similarity in heart size, anatomy and physiology to humans. To address the two aforementioned issues, we first characterized the excitation-ratiometric properties and *ex vivo* performance during ventricular fibrillation (VF) of two near-infrared voltage-sensitive dyes, di-4-ANBDQBS and di-4-ANEQ(F)PTEA, with the use of blebbistatin. On the basis of these results, we built and tested *ex vivo* an optical mapping system using fibre-optic technology and voltage ratiometry without the use of blebbistatin. We then established an intracoronary dye-loading procedure *in vivo* and validated systems that perform ratiometric optical mapping of both induced VF episodes, and APs and activation waves during electrical pacing. Finally, we conducted comprehensive toxicity analyses following percutaneous intracoronary dye injection.

2. Methods

A detailed description of the different Methods sections is provided in the Supplementary material online.

2.1 Study design

We used three different animal groups (large-white pigs, 60–80 kg) as follows: Group I ($n = 14$) consisted of pigs undergoing cardiac excision to characterize the ratiometric properties of di-4-ANBDQBS and di-4-ANEQ(F)PTEA, and to develop optical mapping instrumentation for imaging the contracting heart; Group II ($n = 18$) consisted of pigs undergoing open-chest surgery and percutaneous dye loading into the left anterior descending (LAD) coronary artery to test and validate instrumentation from Group I, as well as to measure deterioration of fluorescence signals over time; and Group III ($n = 12$) consisted of pigs undergoing a minimally invasive percutaneous approach to test dye-related toxicity in the vital organs. All surgical procedures (Group I and Group II animals) were performed under general anaesthesia. Pigs were pre-medicated with a combination of intramuscular Xylazine (2 mg/kg i.m.) and Midazolam (0.5 mg/kg i.m.). Anaesthesia was induced with intravenous Ketamine (20 mg/kg i.v.). After intubation animals were mechanically ventilated and anaesthesia was maintained by a combination of Fentanyl (0.010 mg/kg/h i.v.) and Sevoflurane (2.5%). In interventional procedures (Group III animals), anaesthesia was maintained with continuous intravenous infusion of Ketamine (2 mg/kg/h), Fentanyl (0.005 mg/kg/h i.v.), and Midazolam (0.2 mg/kg/h) to avoid any bias in toxicity assessment related to the cardio-protective effects of Sevoflurane administration.[16] Pigs were euthanized with thiopental (10 mg/kg iv).

The experimental studies were conducted in accordance with institutional guidelines and regulations [National (ECC/566/2015, RD53/2013) and European (2010/63/EU) guidelines for the care and use of laboratory animals]. All *in vivo* experimental procedures were evaluated and granted by the Institutional Animal Care and Use Committee (IACUC) of CNIC and the Local Competent Authority.

2.2 Ratiometric optical mapping in the Langendorff-perfused pig heart

Excised hearts were cleaned, cannulated through the aorta and then connected to a constant-flow Langendorff-perfusion apparatus as reported elsewhere.[12] First, three pig hearts were used to investigate the ratiometric properties of two near-infrared voltage-sensitive dyes, di-4-ANBDQBS and di-4-ANEQ(F)PTEA (University of Connecticut School of Medicine, Farmington, CT, USA) optimized for imaging blood-perfused tissue.[17,18] After an initial 20 min of perfusion following cannulation, the dye was injected at a short distance upstream from the aortic cannula for coronary perfusion. Hearts were loaded with 750 µL (di-4-ANBDQBS) or 500 µL (di-4-ANEQ(F)PTEA) of stock dye solution (10 mg of di-4-ANBDQBS/di-4-ANEQ(F)PTEA dissolved in 3 mL of pure ethanol) diluted in 10 mL of Tyrode's solution, delivered slowly over a 1-min period, without recirculation. After dye loading, the perfusate was replaced with fresh Tyrode's solution containing 10 µM blebbistatin (part #: 674289-55-5; Cayman Chemical Company, Ann Arbor, MI, USA) to minimize contraction.

For imaging, we used two red and two blue light-emitting-diodes (LEDs; part #: CBT-90 Red and CBT-90 Blue; Luminus Devices Inc., Woburn, MA, USA) to excite dye-loaded tissue (*Figure 1A*). The excitation light from each LED was passed through a plano-convex lens (L1 and L2; part #: LA1951; Thorlabs Inc., Newton, NJ, USA) and an excitation filter. Various red and blue excitation filters were used to optimize excitation-ratiometry measurements (i.e. to maximize alterations in emission intensity of opposite polarity). In the adult pig myocardium, we found a substantial shift for both di-4-ANBDQBS and di-4-ANEQ(F)PTEA at ~640 nm vs. ~480 nm (F1 and F2; part #: ZET642/20X passing 632–652 nm and AT480/30X passing 465—495 nm Chroma Technology Corp, Bellows Falls, VT, USA). Dichroic mirrors were used to merge the red and blue lights into one path (D1; part #: T505LPXR passing above 505 nm and reflecting below 505 nm; Chroma Technology Corp.). Fluorescence emission light from the heart was passed through a custom-made emission filter (F3; part #: ET700LP passing above 700 nm; Chroma Technology Corp.) and then collected with a

fast camera lens (L3; part #: DO-1795; Navitar Inc., Rochester, NY, USA). Fluorescence images were taken with a high-speed electron-multiplying charge-coupled device camera running at 400/500 fps (Evolve 128 EMCCD camera; 128 × 128 pixels; Photometrics, AZ, USA). Excitation ratiometry was achieved by synchronizing the red and blue LEDs with the camera frame exposure.

Seven pig hearts were used to test ratiometric optical mapping in the isolated Langendorff-perfused heart loaded with di-4-ANBDQBS ($n = 2$) or di-4-ANEQ(F)PTEA ($n = 5$) without the use of blebbistatin. The optical mapping system outlined in *Figure 1A* was modified to image fluorescence via an optical-fibre array pressed against the epicardial surface (*Figure 1B*). A 4 × 4 array (interfibre distance: 4 mm) of 1500 µm plastic optical fibres was constructed (part #: 02-535; Edmund Optics Inc., Barrington, NJ, USA) and an additional dichroic mirror was used to merge the excitation and emission light into one path (D2; part #: FF685-Di02 passing above 685 nm and reflecting below 685 nm; Semrock Inc., Rochester, NY, USA). Both excitation and emission lights were transmitted down the same optical fibre. Sample optical recordings were also obtained with a catheter-compatible 500 µm plastic optical fibre (part #: 02-532; Edmund Optics Inc.) to increase the translational impact. To zoom in on the proximal end of the smaller fibre, an additional lens was used (L3; part #: DO-1795; Navitar Inc.). Furthermore, the pig hearts loaded with di-4-ANEQ(F)PTEA were used to measure the changes in AP duration (APD) and conduction velocity (CV) due to excitation-contraction uncoupling with blebbistatin.

2.3 Animal preparation for *in vivo* optical mapping

All animals underwent open-chest surgery to expose the ascending aorta and the anterior region of the heart. An electrosurgical blade was used to seal blood vessels for the purpose of haemostasis, which was confirmed to be stable for 15 min before the administration of a single bolus of unfractionated heparin (130 IU/kg i.v.) at the onset of percutaneous coronary instrumentation. Then, an AL-2 6-French guiding catheter was used to cannulate the main left coronary artery, while coronary anatomy was examined via two angiographic projections. The tip of the catheter was positioned into the proximal LAD coronary artery with the use of a 0.014-inch guide. Dye loading was tested using two strategies:

(1) Dye loading in the absence of coronary blood flow ($n = 5$): An occlusion balloon catheter (Helios, LightLab Imaging Inc., Westford, MA, USA) was positioned and inflated at the origin of the LAD coronary artery. The internal lumen of the balloon was used to inject 1.5 mL of stock dye solution diluted in 30 mL of saline and then delivered slowly over a 40-s period. A continuous infusion of amiodarone (100 mg/h) was administered 15 min before balloon occlusion and stopped 5 min after deflating the balloon to decrease the risk of ventricular arrhythmia.

(2) Dye loading in the presence of regular coronary blood flow ($n = 13$): Di-4-ANBDQBS ($n = 4$) was injected using the same dye mixture over a 40-s period. Di-4-ANEQ(F)PTEA ($n = 9$) loading was performed using 1 mL of stock dye solution diluted in 30 mL of saline and then delivered slowly over a 50-s period. No amiodarone perfusion was used with this approach.

The ratiometric optical mapping systems developed for isolated Langendorff-perfused heart preparations were applied *in vivo* following dye injection (*Figure 1C* and *D*).

2.4 Toxicity assessment protocol

Group III animals were divided into three subgroups: (i) di-4-ANBDQBS+solvent injection ($n = 4$), (ii) di-4-ANEQ(F)PTEA+solvent injection ($n = 4$), and (iii) solvent injection ($n = 4$). Intracoronary dye delivery was performed in the same manner as dye loading in the presence of coronary blood flow. Solvent injection was performed using 1.5 mL of pure ethanol (dye solvent) diluted in 30 mL of saline and delivered over a 40-s period. Electrocardiogram (ECG) recordings (see Supplementary material online, *Figure S1*), blood pressure, and pulsioximetry were digitally monitored and acquired at 1 kHz throughout the procedure and for 30 more minutes thereafter (LabSystem-Pro recording system, Boston Scientific, Lowell, MA, USA).

All animals underwent blood testing to obtain toxicity biomarkers related to vital organs using the following sequential timeline: baseline (30 min before the procedure), 30 min, 90 min, 12 h, 24 h, 48 h, 72 h, 7 days and 10 days after coronary dye/solvent injection.

Cardiac magnetic resonance (CMR) studies were performed to determine any overt structural and functional alterations at baseline, 90 min after dye/solvent injection and after 10 days as a follow-up. All studies were performed using a Philips Achieva 3T-Tx whole-body scanner (Philips Healthcare, Best, The Netherlands) equipped with a 32-element phased array cardiac coil. The baseline protocol included Cine, T2 GraSE and T1 mapping sequences without contrast administration. CMR sequences after 90 min and 10 days also included isotropic 3D delayed-enhancement and post-contrast T1 mapping to assess diffuse cardiac damage due to dye/solvent injection.

2.5 Statistical analysis

All statistical comparisons were performed in hearts loaded with di-4-ANEQ(F)PTEA. Ratiometric optical signals for APD and CV comparisons were obtained from four fibres per heart. APD values used were the average of APD_{90} measurements of five consecutive APs during electrical pacing at 400 ms cycle length (CL). The Wilcoxon Signed Rank test was used for statistical comparisons before and after blebbistatin perfusion. The Mann–Whitney *U* test was used for statistical comparisons between *in vivo* and *ex vivo* data. A two-way repeated measures analysis of variance (ANOVA) was used for toxicity comparisons among subgroups over the follow-up period. Differences were considered statistically significant at $P < 0.05$.

3. Results

3.1 Ratiometric properties of di-4-ANBDQBS and di-4-ANEQ(F)PTEA

Our prior experience in Langendorff-perfused pig heart experiments showed that the near-infrared 'second-generation' voltage-sensitive dye, di-4-ANBDQBS, loads easily and without the use of additional agents such as pluronic F-127.[18] Hence, di-4-ANBDQBS was used for the initial phase of this study. After an initial round of *ex vivo* and *in vivo* experiments with di-4-ANBDQBS, we transitioned to using a near-infrared 'third-generation' fluorinated voltage-sensitive dye, di-4-ANEQ(F)PTEA, with improved photostability and solubility.[17] An experimental flow-chart is shown in *Figure 2A*.

Ratiometric dyes characteristically display a spectral shift in their excitation or emission spectra. After arresting contraction with blebbistatin, we found that both di-4-ANBDQBS and di-4-ANEQ(F)PTEA showed a substantial shift at ~480 nm vs. ~640 nm (*Figure 2B*). The numerator and denominator AP signals were obtained by exciting tissue at ~480 and ~640 nm, respectively. The same AP led to alterations in emission intensity of opposite polarity. Normalized transmembrane voltage fluorescence intensity maps, using the ratio signal enabled the tracking and

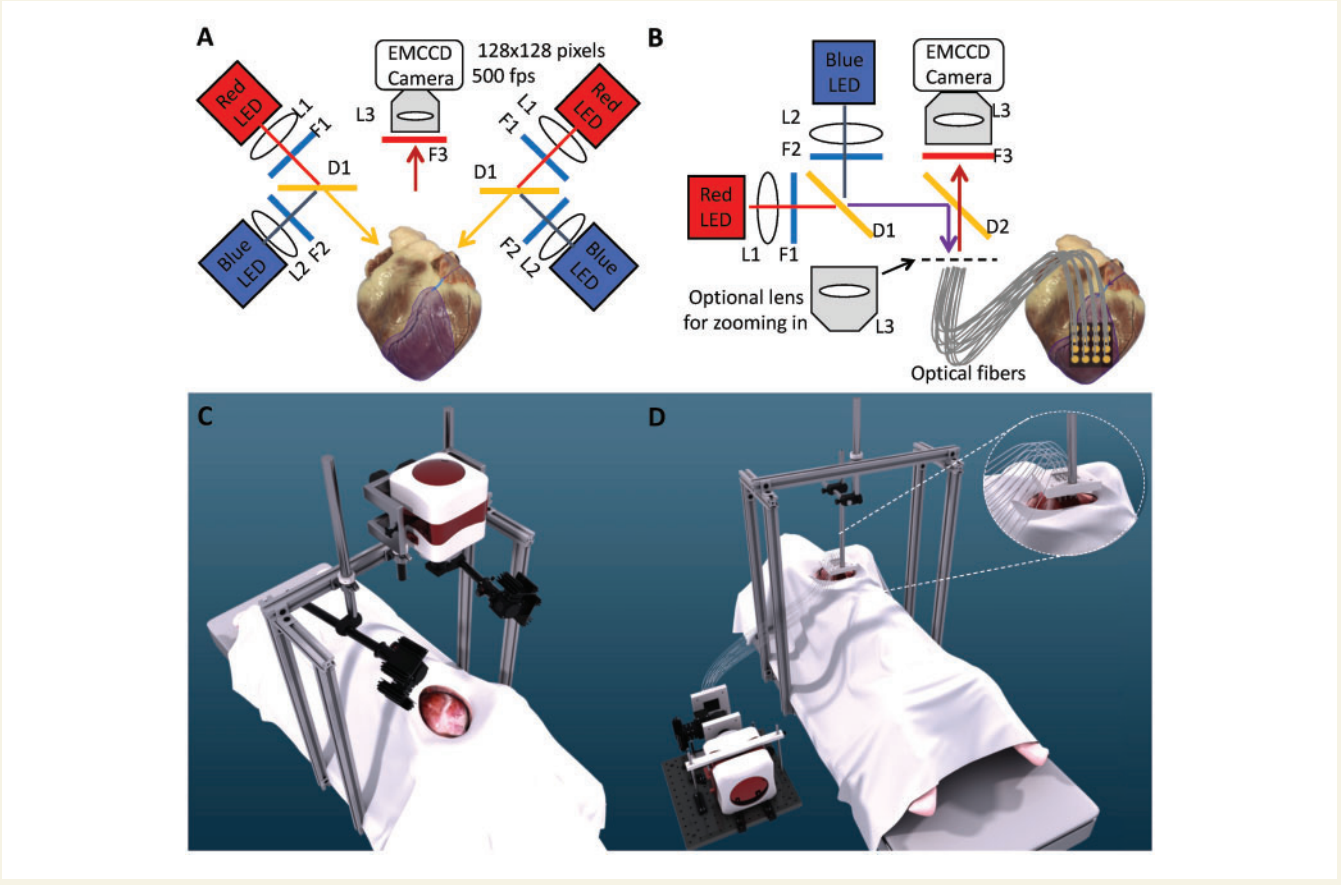

Figure 1 *In vivo* optical mapping systems. (*A*) Schematic representation of the system built to optically map the exposed heart in the open-chest pig during dye loading and ventricular fibrillation (dye-loading region highlighted purple). (*B*) Schematic representation of the modified system using an optical-fibre array to measure action potentials during regular contraction. (*C*) 3D representation of the system in (*A*) during an *in vivo* experiment. (*D*) 3D representation of the system in (*B*) during an *in vivo* experiment.

visualization of the activation and repolarization fronts propagating across the epicardium (*Figure 2C* and see Supplementary material online, *Movies S1* and *S2*). Ratiometric imaging of complex activation patterns during VF also showed alterations in emission intensity of opposite polarity for each excitation potential (*Figure 2D* and see Supplementary material online, *Movies S3* and *S4*). The ratio signal also enabled the generation of dominant frequency (DF) maps (*Figure 2D*).

3.2 Voltage ratiometry *ex vivo* enables optical mapping in the contracting heart

Since motion artefacts display a similar change and the same polarity in fluorescence for ~480 and ~640 nm excitations, taking the ratio of the numerator to denominator signal has the potential to significantly reduce motion artefacts in the contracting heart not arrested with blebbistatin. A experimental flow-chart is shown in *Figure 3A*.

A 2D optical-fibre array (4 × 4) was pressed against the epicardial surface of the Langendorff-perfused pig heart (*Figure 3B* and see Supplementary material online, *Movie S5*) after di-4-ANBDQBS/di-4-ANEQ(F)PTEA loading. Sample numerator and denominator AP signals are shown in *Figure 3B* during 400 ms CL pacing. Sample activation maps illustrating wave front propagation are also shown in *Figure 3C* (see Supplementary material online, *Movie S6*) (di-4-ANEQ(F)PTEA). Although the rapid increase (numerator) and decrease (denominator) corresponding to the phase-zero depolarization were discernible, repolarization signals were highly distorted by motion artefacts. Taking the ratio of these signals significantly reduced artefacts, uncovering the AP repolarization (*Figure 3B*).

In Langendorff-perfused hearts loaded with di-4-ANEQ(F)PTEA ($n = 5$), ratiometric optical-fibre data before and after 30 min of blebbistatin administration in the perfusate (*Figure 3B* and *C*) showed a significant prolongation of APD [median (inter-quartile range), APD_{90} 192 (182–233) ms vs. 227 (210–254) ms, respectively; $P = 0.031$, *Figure 3D*] and a decrease in CV [51 (41–64) cm/s vs. 38 (32–48) cm/s, respectively; $P = 0.031$, *Figure 3E*]. A highly flexible and catheter-compatible plastic optical fibre (500 μm diameter) also showed APs in the contracting heart with minimal motion artefacts (*Figure 3F*).

3.3 Di-4-ANBDQBS and di-4-ANEQ(F)PTEA loading *in vivo*

Fluorescence imaging of the exposed heart was carried out at relatively high frame rates (300 fps) to capture fluorescence coronary angiograms and to assess the efficacy of dye-loading protocols. A higher spatial

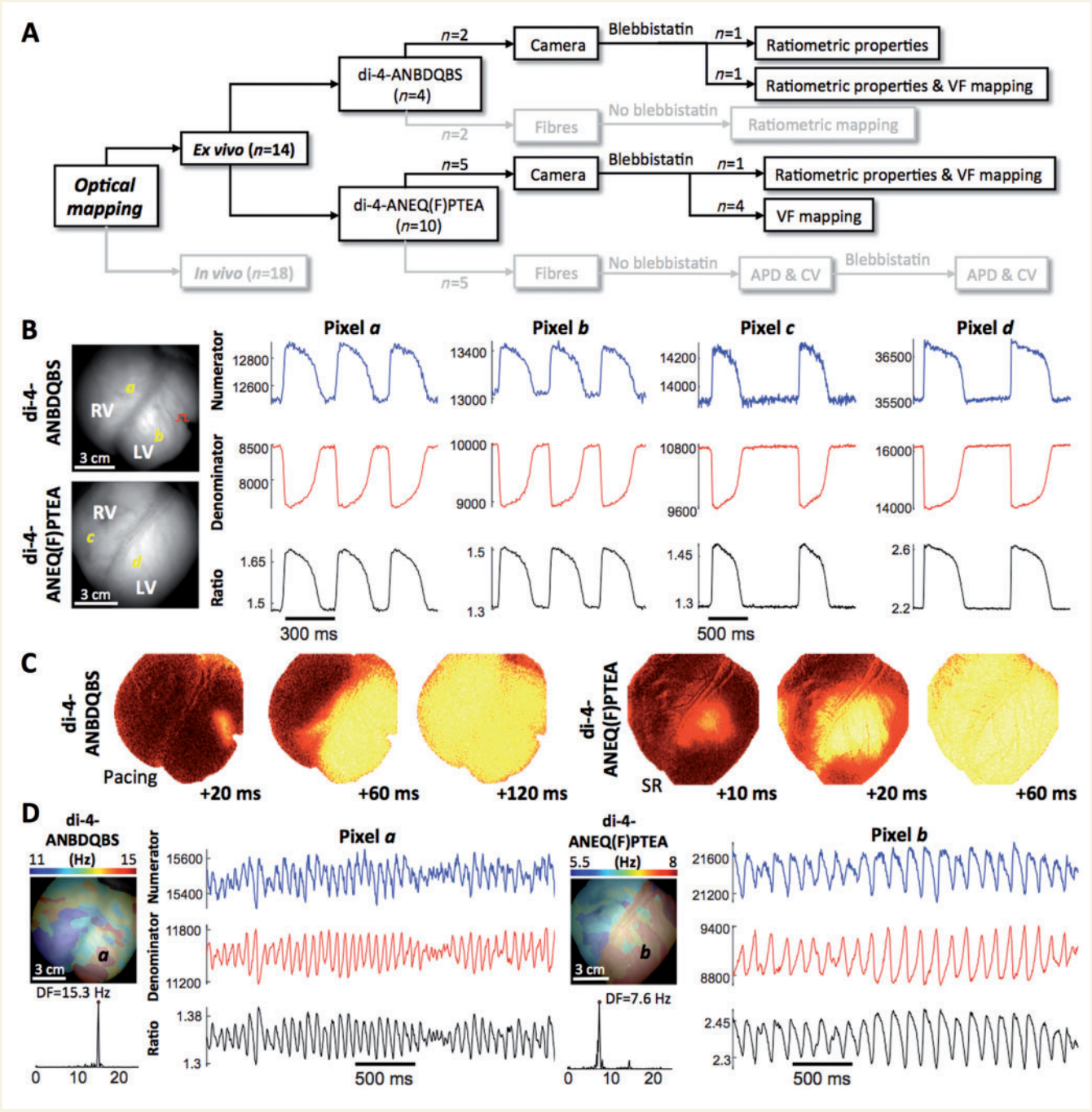

Figure 2 Excitation ratiometry of di-4-ANBDQBS and di-4-ANEQ(F)PTEA in the isolated pig heart with excitation-contraction uncoupled. (*A*) Flowchart of optical mapping experiments represented in the figure. (*B*) Action potential (AP) signals at sites 'a', 'b' (di-4-ANBDQBS), 'c,' and 'd' (di-4-ANEQ(F)PTEA) on the epicardial surface of the heart obtained by exciting the tissue at ~480 nm (numerator; blue) and ~640 nm (denominator; red). The ratio of the numerator to denominator signal is shown in black (stimulation site: red square pulse). (*C*) Time series of normalized transmembrane voltage fluorescence intensity maps (using ratio signals) during point electrical pacing (500 ms CL) (di-4-ANBDQBS) and sinus rhythm (di-4-ANEQ(F)PTEA). (*D*) DF maps during VF using di-4-ANBDQBS (left panels) and di-4-ANEQ(F)PTEA (right panels). Sample AP signals and DF values are shown at sites 'a' (di-4-ANBDQBS) and 'b' (di-4-ANEQ(F)PTEA). AP signals illustrate irregular electrical activity and alterations in emission intensity of opposite polarity. Signals are in arbitrary fluorescence units. DF, dominant frequency; LV, left ventricle; RV, right ventricle; SR, sinus rhythm.

resolution CMOS camera (complementary metal–oxide–semiconductor) was used instead of the EMCCD camera (*Figure 1C*) and only the red LEDs were used to excite the exposed cardiac tissue during dye-loading procedures (see Supplementary material online, *Movie S7*). Efficacy was assessed qualitatively by looking at live fluorescence videos of the dye-loaded cardiac tissue at high frame rates (300 fps) and detecting sudden decreases in emission intensity corresponding to the phase-zero depolarization (see Supplementary material online, *Movie S8*).

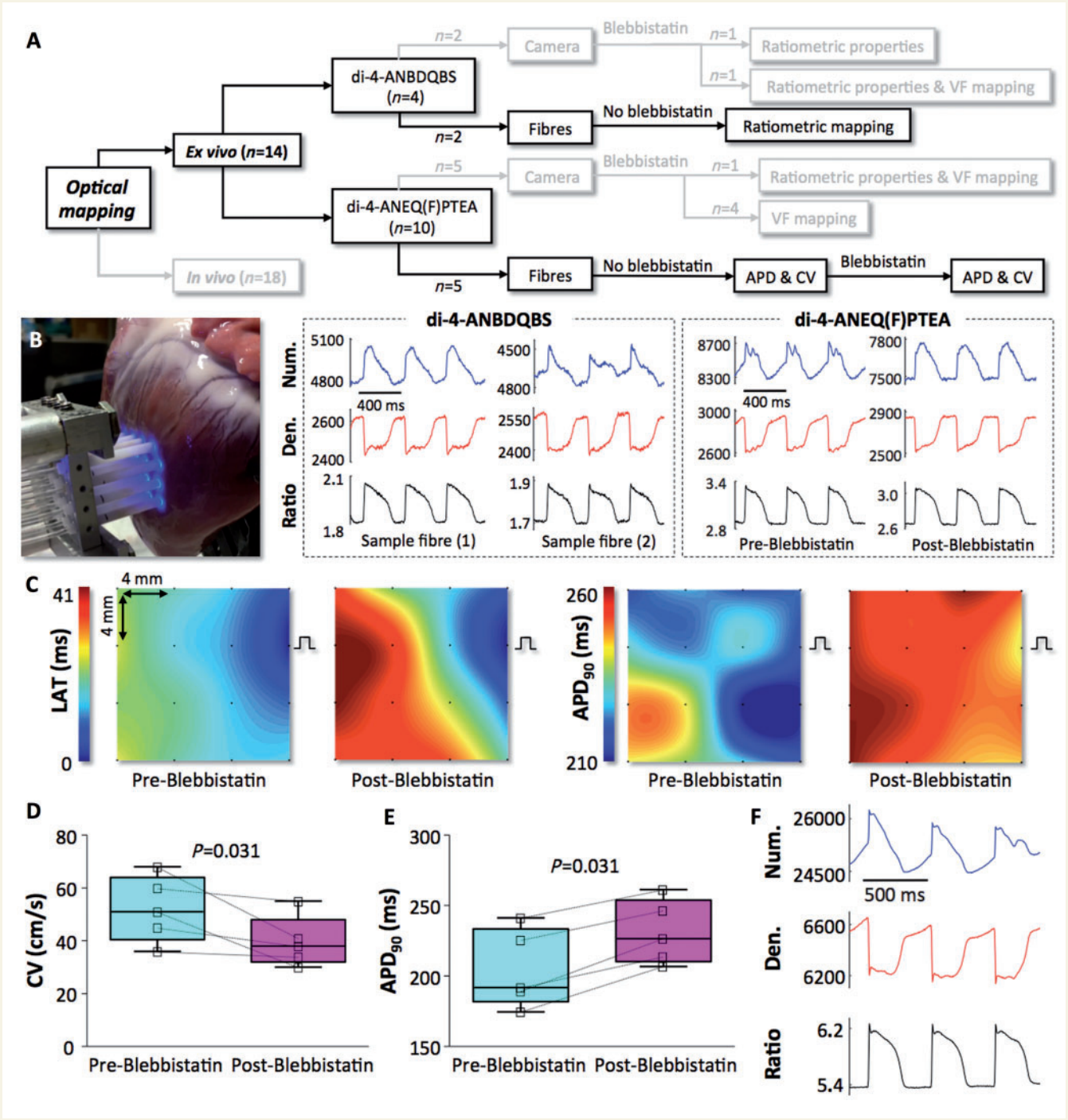

Figure 3 *Ex vivo* optical fibre-based excitation ratiometry of di-4-ANBDQBS and di-4-ANEQ(F)PTEA in contracting tissue. (*A*) Flow-chart of optical mapping experiments represented in the figure. (*B*) 2D optical-fibre array pressed against the surface of a Langendorff-perfused pig heart (left panel). Numerator (blue), denominator (red) and ratio (black) action potential signals from two sample fibres using di-4-ANBDQBS (middle panel), and before and after blebbistatin using di-4-ANEQ(F)PTEA (right panel). (*C*) Sample activation maps illustrating propagation of the wavefront (left panel) and APD maps (right panel) before and after blebbistatin in the perfusate. Stimulation sites (black square pulses) are shown relative to the fibre array. (*D, E*) APD (*D*) and CV (*E*) comparisons (Wilcoxon Signed Rank test) before and after blebbistatin in the perfusate. Five hearts and four sample fibres per heart were included in the analysis. (*F*) AP signals from a 500 μm fibre, demonstrating motion artefact cancellation. Signals are in arbitrary fluorescence units. APD, action potential duration; CV, conduction velocity; LAT, local activation time.

Dye-loading was possible both in the absence of and in the presence of regular coronary blood flow (*Figure 4A* and *B*). However, coronary occlusion during dye loading led to VF requiring direct-current shock in three out of five pigs (see experimental flow-chart in *Figure 5A*). Therefore, subsequent experiments were performed using the dye-loading protocol in the presence of regular coronary blood flow. Importantly, although both di-4-ANBDQBS and di-4-ANEQ(F)PTEA loaded easily *ex vivo*, we found that di-4-ANEQ(F)PTEA loaded significantly more easily *in vivo*.

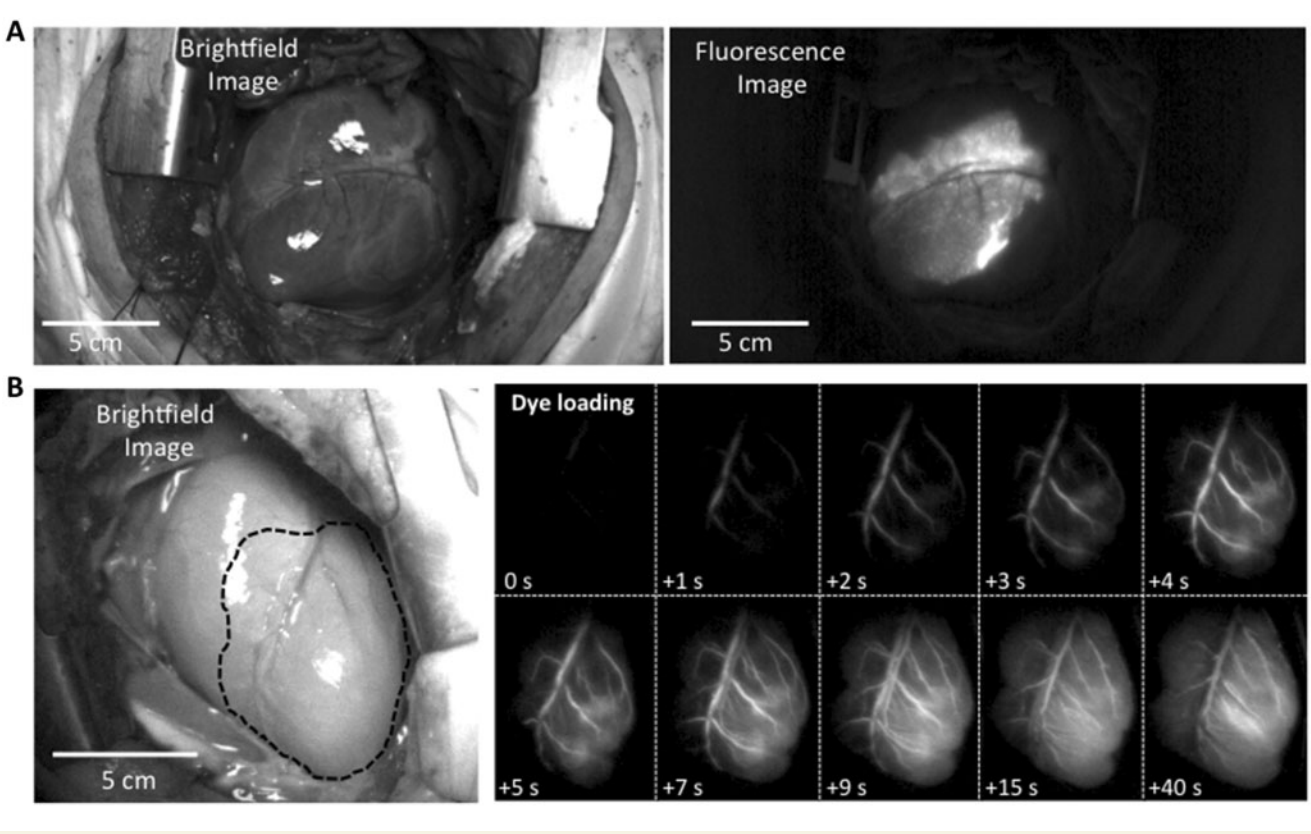

Figure 4 *In vivo* dye loading. (*A*) Left panel: Brightfield image of a sample heart loaded using balloon occlusion of the LAD coronary artery. Right panel: Fluorescence image of the same heart using red LED excitation (~640 nm). (*B*) Left panel: Brightfield image of another sample heart with the dye-loading region delineated by the black dashed line. Right panels: Snapshots of a fluorescence coronary angiogram recorded at 300 fps with a high-resolution CMOS camera during dye loading in the presence of regular coronary blood flow.

3.4 Voltage ratiometry *in vivo* enables optical mapping of VF dynamics

Without excitation-contraction uncoupling, motion of the contracting heart was expectedly substantial. To image the propagation of activation fronts, electrical stimulation was performed at relatively high frequencies (300 ms CL) to reduce motion (an experimental flow-chart is shown in *Figure 5A*). Although the tissue translation accompanying each contraction led to substantial motion artefacts, ratiometry alone using both di-4-ANBDQBS and di-4-ANEQ(F)PTEA could significantly reduce these artefacts (*Figure 5B*), permitting the tracking of wavefront propagation and the generation of activation maps from the stimulation site (*Figure 5C* and *D*; see Supplementary material online, *Movies S9* and *S10*). During VF, however, motion was significantly reduced and ratiometric optical mapping eliminated most of the motion artefacts, which enabled the generation of DF maps (*Figure 5E*). Moreover, voltage ratiometry also allowed high-resolution tracking of VF dynamics (see Supplementary material online, *Movie S11* and *S12*). DF analysis showed significantly higher DF_{max} values in *ex vivo* Langendorff-perfused hearts ($n = 5$) compared with *in vivo* episodes ($n = 4$) upon VF induction [9.3 (8.5–10.6) Hz vs. 7.4 (6.4–8.7) Hz; $P = 0.032$]. Conversely, *in vivo* episodes showed a statistical trend to a higher singularity point density upon VF induction [0.77 (0.53–0.98)% vs. 0.41 (0.36–0.57)%; $P = 0.064$, *Figure 5F* and see Supplementary material online, *Movies S13* and *S14*].

3.5 Optical fibres enable *in vivo* optical mapping of organized rhythms

Although ratiometry substantially reduces motion artefacts (*Figure 5B*), far-field imaging of organized rhythms cannot generate accurate APD maps due to translational motion. Therefore, the fibre-based imaging system outlined in *Figure 1B* and *D* was constructed to obtain AP recordings during organized electrical activity. An experimental flow-chart is shown in *Figure 6A*. The distal optical-fibre ends were pressed against the heart surface (*Figure 6B* and see Supplementary material online, *Movie S5*) to measure wave propagation dynamics and APs in strongly contracting hearts during pacing. Sample numerator-, denominator-, and ratio-action-potential signals using both di-4-ANBDQBS and di-4-ANEQ(F)PTEA are shown in *Figure 6B*. Sample activation and APD maps are also shown in *Figure 6C*. Synchronized ECG and blood pressure measurements could be also obtained during *in vivo* optical mapping (see Supplementary material online, *Figure S2*).

Ratiometric optical-fibre data during pacing at 400 ms CL *in vivo* showed significantly faster CV [120 (63–138) cm/s vs. 51 (41–64) cm/s; $P = 0.032$, *Figure 6D*] and a statistical trend to longer APD [APD_{90} 242 (217–254) ms vs. 192 (182–233) ms; $P = 0.095$, *Figure 6D*] compared with *ex vivo* measurements before blebbistatin perfusion.

To quantify the signal decay *in vivo*, we measured the signal-to-noise ratio [SNR= (AP Amplitude)/(SD during diastolic intervals)] decay rate

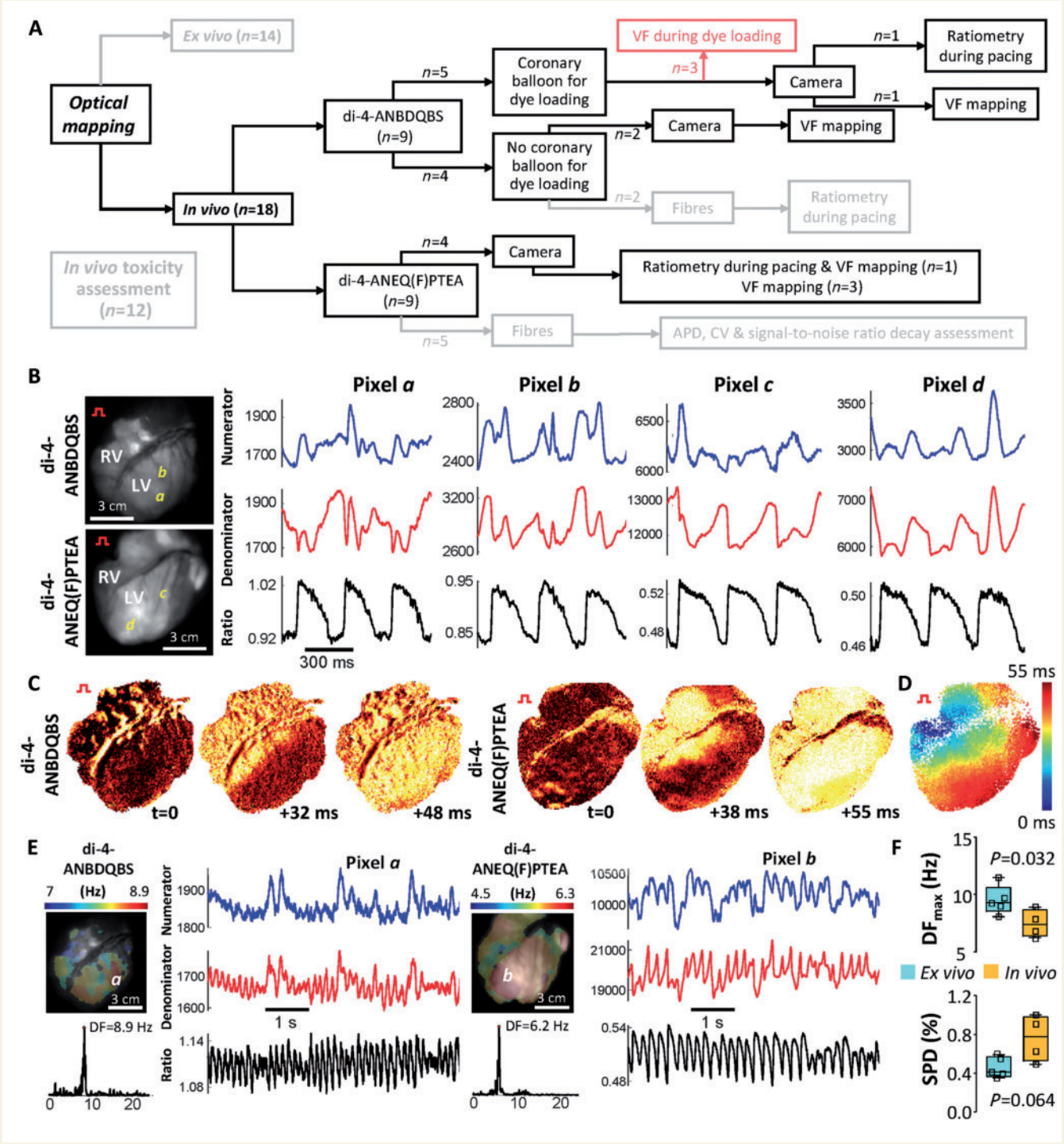

Figure 5 *In vivo* optical mapping of paced rhythms and ventricular fibrillation (VF). (*A*) Flow-chart of optical mapping experiments represented in the figure. (*B*) Action potential (AP) signals at sites 'a', 'b' (di-4-ANBDQBS), 'c,' and 'd' (di-4-ANEQ(F)PTEA) on the epicardial surface of the heart obtained by exciting the tissue at ~480 nm (numerator; blue) and ~640 nm (denominator; red). The ratio of the numerator to denominator signal is shown in black (stimulation sites: red square pulses). Despite the substantial motion, ratiometric optical mapping could detect the AP upstroke. (*C*, *D*) Time series of normalized transmembrane voltage fluorescence intensity maps and activation map (using ratio signals) during point electrical pacing (300 ms CL). (*E*) DF maps during VF using di-4-ANBDQBS (left panels) and di-4-ANEQ(F)PTEA (right panels). Sample AP signals and DF values are shown at sites 'a' (di-4-ANBDQBS) and 'b' (di-4-ANEQ(F)PTEA). AP signals illustrate irregular electrical activity during VF. Signals are in arbitrary fluorescence units. (*F*) DF and SPD comparisons (Mann–Whitney *U* test) between *in vivo* ($n = 4$) and *ex vivo* ($n = 5$) VF episodes. DF, dominant frequency; LV, left ventricle; RV, right ventricle; SPD, singularity point density; VF, ventricular fibrillation.

over a 50-min period following di-4-ANEQ(F)PTEA injection. Fitting the data points to a single-term exponential model (*Figure 6E*), the average decay rate for four animals was 0.0671 ± 0.0090 min^{-1}. Reloading with di-4-ANEQ(F)PTEA showed that the SNR fully recovered (*Figure 6F*). Conversely, the SNR decay rate in the Langendorff-perfused heart was much slower 0.006836 min^{-1} (see Supplementary material online, *Figure S3*).

3.6 Intracoronary di-4-ANBDQBS/di-4-ANEQ(F)PTEA injection does not induce toxicity to the vital organs

A flow-chart of the toxicity analyses is shown in *Figure 7A*. Continuous ECG monitoring from baseline to 30 min after dye/solvent injection showed no signs of di-4-ANBDQBS/di-4-ANEQ(F)PTEA-related cardiac toxicity. Heart rates were stable throughout the recording period in all three subgroups (see Supplementary material online, *Figure S4A*). Flushing with saline before dye/solvent injection showed transient negative T waves on the ECG, with the heart fully recovering within 1 min. The same effect was observed during dye/solvent injection (*Figure 7B*). ECG intervals (PR, QRS complex, and corrected QT interval) did not show statistically significant differences among subgroups *(Figure 7C* and *D*; see Supplementary material online, *Figure S4B*). Invasive blood pressure monitoring revealed transient hypotension (severe in two animals) after di-4-ANBDQBS injection, which was not observed after di-4-ANEQ(F)PTEA or solvent injection (*Figure 7E*).

Cardiac, brain, liver, and kidney biomarkers did not show statistically significant differences among subgroups nor any signs of overt toxicity at any time point (*Figure 7F* and see Supplementary material online, *Figure S5*). A very mild increase in Troponin I was observed at 12 and 24 h after dye/solvent injection, though not reaching the infarct threshold level currently established for percutaneous interventional procedures (*Figure 7F*). Similarly, none of the other blood and plasma biomarkers, sodium, potassium, and chlorine levels showed any overt alterations or statistically significant differences among subgroups (see Supplementary material online, *Figure S6*).

Tissue characterization using CMR imaging did not show acute/late signs of myocardial oedema, scar tissue development nor deterioration of the left ventricular ejection function in all three subgroups (*Figure 7G, H* and see Supplementary material online, *Figures S7* and *S8*).

4. Discussion

Here, we reported measurements of cardiac APs and wave propagation dynamics *in vivo* using optical methods, enabling the acquisition of high spatiotemporal resolution cardiac electrophysiology information. Our experimental method was applied to a pig model using near-infrared voltage-sensitive dyes, which were injected percutaneously into the regular coronary blood flow. The presented series of experiments and dye toxicity studies support our aim to make *in vivo* optical mapping a standard experimental method that can lead to results with strong clinical implications.

Cardiac optical mapping is primarily based on high-speed fluorescence imaging or recording of synthetic voltage-sensitive dyes bound to cardiomyocyte plasma membranes. The high-speed spectral shift due to changes in transmembrane voltage permits the accurate measurement of APs.[19] Optical mapping provides a number of advantages over conventional extracellular recordings,[20] foremost is the ability to directly track AP propagation at the cellular level, leading to greater spatial resolution at the tissue level.[2,14] However, the motion accompanying each heart beat affects signal fidelity. This has led to the use of mechanical uncouplers (e.g. blebbistatin), and heart immobilization techniques during optical mapping experiments. Although some researchers have reported that 10 μM blebbistatin perfusion has no effect on AP morphology in rabbit cardiac tissue,[21] others have documented significant prolongation of the APD and have speculated decreases in CV at just 5 μM blebbistatin perfusion.[22] Furthermore, the use of excitation-contraction uncouplers like blebbistatin precludes the simultaneous measure of contractility, an important physiological parameter. Our study was not designed to address the effects of blebbistatin on APD and CV. The observed changes in APD and CV when using blebbistatin might not be a specific effect of the drug, but rather a consequence of the metabolic state of the heart when ATP is abundant due to contraction inhibition. In addition, APD prolongation may be time-dependent (time-matched control experiments were not performed in our study). The observed decrease in CV during pacing may also be a direct effect of APD prolongation.

Of the imaging methods developed for handling motion artefacts during *ex vivo* optical mapping studies, ratiometry has been shown to significantly reduce artefacts in AP signals.[23] Its use *in vivo* has not been reported to our knowledge. Furthermore, there have been no published investigations of the ratiometric properties of near-infrared voltage-sensitive dyes developed for blood-perfused cardiac tissue in a clinically relevant animal model like the adult pig. Though di-4-ANEPPS was used in the first and only reported *in vivo* optical mapping study in a large mammal model, ratiometry was not employed and green light was used for dye excitation, which is strongly absorbed by blood.[24] Unlike di-4-ANEPPS, near-infrared voltage-sensitive dyes have optimal excitation wavelengths in cardiac tissue beyond the absorption maximum of haemoglobin and other endogenous chromophores, making its use optimal for deeper tissue probing and optical mapping in blood-perfused myocardium.[18,25] Importantly, our investigation demonstrates that both di-4-ANBDQBS and di-4-ANEQ(F)PTEA display spectral shifts in excitation spectra, with voltage dependence of opposite polarity at ∼480 nm vs. ∼640 nm, corresponding, respectively, to the blue and red wings of the dye excitation spectrum.

Past studies have also investigated the ratiometric properties of di-4-ANEPPS *ex vivo* in the adult pig myocardium, although the technique was not translated to an *in vivo* setting and utilized a more costly implementation requiring two cameras/detectors (i.e. emission ratiometry).[26] The optical mapping systems developed in this study used excitation ratiometry, a single camera and low-cost LED light sources. The use of different excitation wavelengths in excitation ratiometry, though, leads to differences in photon absorption and scattering in cardiac tissue.[27] Our approach enabled us to identify propagation wave fronts and detect APs *in vivo* under different motion conditions. Furthermore, newer dyes, like the di-4-ANBDQBS and di-4-ANEQ(F)PTEA dyes used in this study, have higher voltage sensitivity and are more resistant to photobleaching and cellular internalization.[18]

The open-chest pig animal model, though critical to the development of *in vivo* optical mapping methods and relevant to studying complex patterns of propagation in easily exposed epicardial tissue, involves an invasive procedure that limits its translational impact. Our development and validation of an optical-fibre mapping system was an initial attempt at enabling closed chest procedures. Further development of optical-fibre mapping systems would not only simplify certain aspects of *in vivo* experiments and instrumentation, it would have direct application to clinical settings. The first and seminal *in vivo* optical mapping study in the late

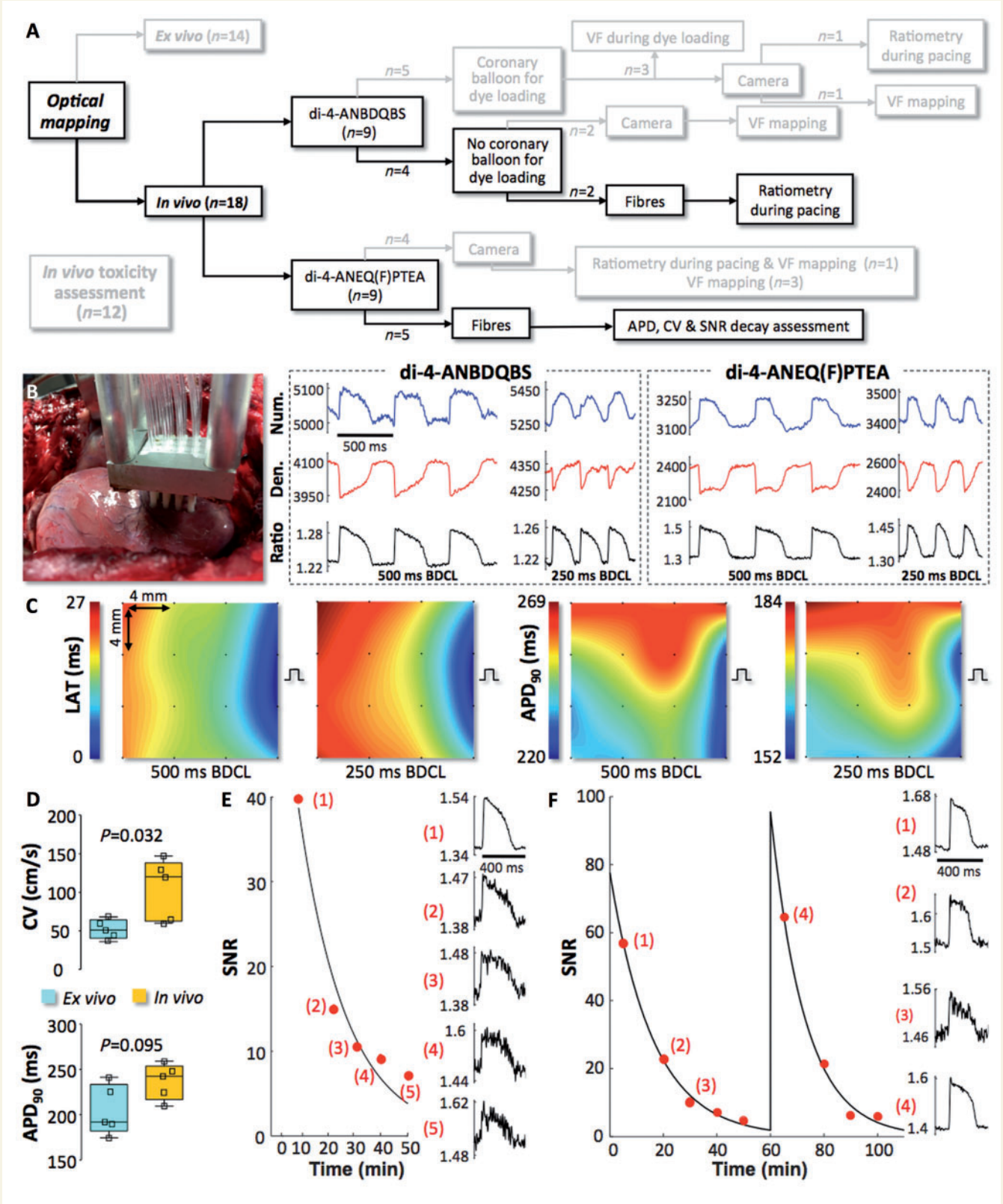

Figure 6 *In vivo* optical-fibre fluorescence recordings. (*A*) Flow-chart of optical mapping experiments represented in the figure. (*B*) Positioning of the optical-fibre array during an experimental procedure (left panel). Sample numerator (blue), denominator (red) and ratio (black) AP signals at 500 and 250 ms BDCLs using di-4-ANBDQBS (middle panel) and di-4-ANEQ(F)PTEA (right panel). (*C*) Sample activation maps illustrating propagation of the wavefront (right panels) and APD maps (left panels) at 500 and 250 ms BDCLs using di-4-ANEQ(F)PTEA. Stimulation sites (black square pulses) are shown relative to the fibre array. (*D*) APD and CV comparisons (Mann–Whitney *U* test) between *in vivo* ($n = 5$) and *ex vivo* ($n = 5$) hearts (four sample fibres per heart). (*E*, *F*) Two sample SNR decays (*E*, *F*) and reloading (*F*) with di-4-ANEQ(F)PTEA. Signals are in arbitrary fluorescence units. APD, action potential duration; BDCL, basic drive cycle length; CV, conduction velocity; LAT, local activation time; SNR, signal-to-noise ratio.

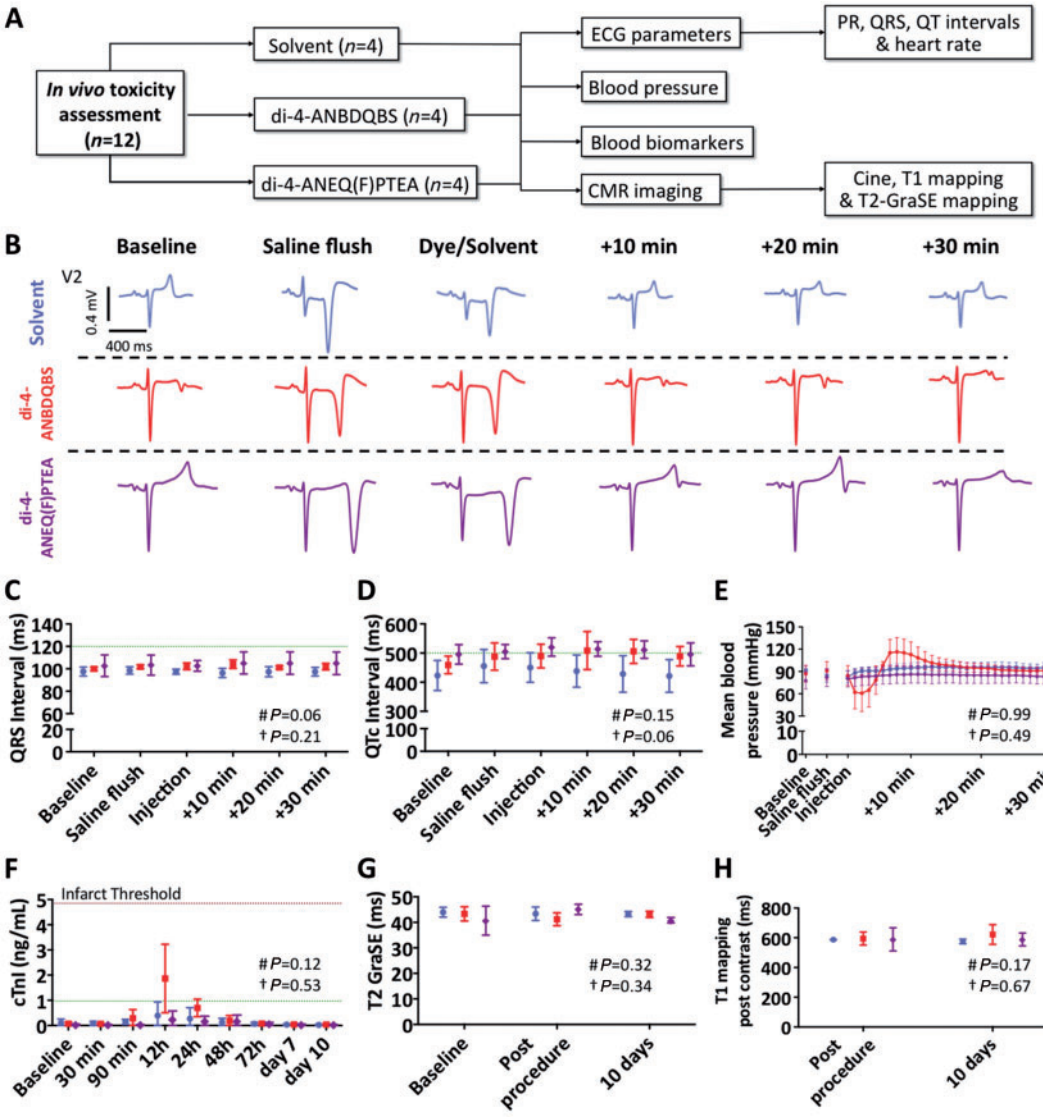

Figure 7 Dye toxicity assessment. (*A*) Flow-chart of the toxicity protocol. (*B*) Sample ECG tracings (lead V2) during the monitoring period in the three subgroups. (*C–F*) QRS complex duration (*C*), corrected QT interval (*D*), mean blood pressure (*E*), and Troponin I (cTnI) (*F*) comparisons among subgroups. The infarct threshold criterion after percutaneous coronary interventions is represented with a brown dashed line (*F*). (*G*, *H*) Comparisons of T2 GraSE (*G*) and post-contrast T1 mapping (*H*) sequences among subgroups. Data are represented as mean and standard deviation, but in (*E*), standard errors of the means are shown because of the large variability in blood pressure measurements. Physiological ranges are represented with green dashed lines. Blue circles: solvent ($n = 4$). Red squares: di-4-ANBDQBS+solvent ($n = 4$). Purple diamonds: di-4-ANEQ(F)PTEA+solvent ($n = 4$). $^{\#}$ and † indicate *P*-values for two-way repeated measures ANOVA of solvent vs. di-4-ANBDQBS ($^{\#}$), and solvent vs. di-4-ANEQ(F)PTEA (†).

1990s also used optical fibres to record APs and propagation dynamics. The voltage-sensitive dye di-4-ANEPPS and a canine animal model were used to demonstrate the feasibility of translating *ex vivo* optical mapping techniques to an *in vivo* setting.[28] Other than one study in a rat animal model,[29] there has been no subsequent published work further developing *in vivo* optical mapping, which we presume was due to technical limitations. For instance, the rat study used a non-physiological cardiopulmonary bypass circuit to offload the blood-pumping work to an external pump. Although this approach would permit the use of heart immobilization techniques, its potential translational application would be very limited and simultaneous measurement of contractility would not be possible. Here, we reported that these technical limitations no longer exist and high-performance optical mapping catheter development is now feasible.[25,30,31] Complemented with the development of higher-performance voltage-sensitive dyes and dye-loading procedures,[17] *in vivo* optical mapping has the potential to open the door to a new era of high-performance mapping in the cardiac electrophysiology field.

In vivo intracoronary dye injection and loading naturally raises concerns regarding toxicity in the heart and other vital organs. Indeed, previous reports using di-4-ANEPPS in isolated cardiomyocytes have documented illumination-induced phototoxicity that could be decreased by adding the antioxidant catalase, suggesting the involvement of a reactive oxygen species during induced-photodynamic damage.[32] Though phototoxicity appears to be less pronounced in whole heart

preparations, the use of the newer dyes has been shown to lead to much smaller effects on APD than the older di-4-ANEPPS dye.[33] But neither isolated cell nor Langendorff-perfused heart preparations can provide toxicity data that can be extrapolated to the *in vivo* setting. As such, we conducted a comprehensive toxicity study, in which intracoronary dye injection did not induce acute nor subacute signs of damage to vital organs (long-term illumination-induced phototoxicity was not tested). Moreover, we did not observe dye-induced pro-arrhythmia during injection. The risk of VF was only present when dye injection was performed in the absence of regular coronary blood flow using balloon occlusion. Severe transient hypotension was the main effect observed during di-4-ANBDQBS injection, though it varied from animal to animal. Hypotension was not observed using di-4-ANEQ(F)PTEA.

We acknowledge that some limitations are still present. Di-4-ANBDQBS, di-4-ANEQ(F)PTEA, and other newly developed near-infrared dyes must be further characterized in both pig and human cardiac tissues.[14,34,35] Both optical spectra and toxicity profiles must be established for existing candidate dyes while new voltage-sensitive dyes are specifically developed for *in vivo* optical mapping. Improvements need to be made in voltage-sensitivity, solubility in aqueous solvents and tissue loading speed. Though toxicity profiling in humans would require approval by international regulatory agencies, recent work using the FDA-approved Indocyanine Green as a voltage-sensitive dye in isolated rabbit hearts may help lower boundaries to testing optimized voltage-sensitive dyes in humans.[36]

Further developments in instrumentation are also needed. For instance, catheters capable of measuring complementary electrical and optical signals may prove useful for different myocardial substrates with complex electrical signal interpretation.[10] The *in vivo* optical mapping techniques reported here, however, can already be used to investigate complex VF episodes after myocardial infarction in clinically relevant animal models. The latter would be difficult to perform with current electrical mapping technologies.[11,37] However, voltage ratiometry during far-field *in vivo* imaging of organized rhythms cannot generate accurate APD nor repolarization maps without implementing further signal processing and motion tracking routines.[38,39]

In conclusion, we have demonstrated an experimental method for performing *in vivo* optical mapping in a pig animal model, addressing issues related to motion artefacts, dye loading, and toxicity. Further development and experimentation may lead to a significant and clinically relevant advance in high resolution *in vivo* mapping of cardiac electrophysiology.

Supplementary material

Supplementary material is available at *Cardiovascular Research* online.

Acknowledgements

We are grateful for technical support provided by the animal facility at CNIC. We also thank the Richard D. Berlin Center for Cell Analysis and Modeling.

Conflict of interest: P.L. is both an owner and employee of Essel Research and Development Inc. P.Y. is both an owner and employee and L.M.L. is an owner of Potentiometric Probes, LLC. The other authors report no conflicts.

Funding

The CNIC is supported by the Ministry of Science, Innovation and Universities and the Pro CNIC Foundation. The CNIC is a Severo Ochoa Center of Excellence (SEV-2015-0505). This study was supported by grants from Fondo Europeo de Desarrollo Regional (CB16/11/00458), the Spanish Ministry of Science, Innovation and Universities (SAF2016-80324-R, PI16/02110, and DTS17/00136), and by the European Commission (ERA-CVD Joint Call [JTC2016/APCIN-ISCIII-2016], grant#AC16/00021). The study was also partially supported by the Fundación Interhospitalaria para la Investigación Cardiovascular (FIC) and the Heart Rhythm section of the Spanish Society of Cardiology. The work at the University of Connecticut was supported by grant EB001963 from the National Institutes of Health.

References

1. Neher E, Sakmann B. Single-channel currents recorded from membrane of denervated frog muscle fibres. *Nature* 1976;**260**:799–802.
2. Gray RA, Jalife J, Panfilov AV, Baxter WT, Cabo C, Davidenko JM, Pertsov AM, Hogeweg P, Winfree AT. Mechanisms of cardiac fibrillation. *Science* 1995;**270**:1222–1223.
3. Horowitz LN, Harken AH, Kastor JA, Josephson ME. Ventricular resection guided by epicardial and endocardial mapping for treatment of recurrent ventricular tachycardia. *N Engl J Med* 1980;**302**:589–593.
4. Narayan SM, Baykaner T, Clopton P, Schricker A, Lalani GG, Krummen DE, Shivkumar K, Miller JM. Ablation of rotor and focal sources reduces late recurrence of atrial fibrillation compared with trigger ablation alone: extended follow-up of the CONFIRM trial. *J Am Coll Cardiol* 2014;**63**:1761–1768.
5. Marchlinski FE, Haffajee CI, Beshai JF, Dickfeld TM, Gonzalez MD, Hsia HH, Schuger CD, Beckman KJ, Bogun FM, Pollak SJ, Bhandari AK. Long-term success of irrigated radiofrequency catheter ablation of sustained ventricular tachycardia: post-approval THERMOCOOL VT trial. *J Am Coll Cardiol* 2016;**67**:674–683.
6. Piers SR, Tao Q, de Riva Silva M, Siebelink HM, Schalij MJ, van der Geest RJ, Zeppenfeld K. CMR-based identification of critical isthmus sites of ischemic and nonischemic ventricular tachycardia. *JACC Cardiovasc Imaging* 2014;**7**:774–784.
7. Sasaki T, Miller CF, Hansford R, Yang J, Caffo BS, Zviman MM, Henrikson CA, Marine JE, Spragg D, Cheng A, Tandri H, Sinha S, Kolandaivelu A, Zimmerman SL, Bluemke DA, Tomaselli GF, Berger RD, Calkins H, Halperin HR, Nazarian S. Myocardial structural associations with local electrograms: a study of postinfarct ventricular tachycardia pathophysiology and magnetic resonance-based noninvasive mapping. *Circ Arrhythm Electrophysiol* 2012;**5**:1081–1090.
8. Ndrepepa G, Caref EB, Yin H, el-Sherif N, Restivo M. Activation time determination by high-resolution unipolar and bipolar extracellular electrograms in the canine heart. *J Cardiovasc Electrophysiol* 1995;**6**:174–188.
9. Haws CW, Lux RL. Correlation between in vivo transmembrane action potential durations and activation-recovery intervals from electrograms. Effects of interventions that alter repolarization time. *Circulation* 1990;**81**:281–288.
10. Anter E, Tschabrunn CM, Buxton AE, Josephson ME. High-resolution mapping of postinfarction reentrant ventricular tachycardia: electrophysiological characterization of the circuit. *Circulation* 2016;**134**:314–327.
11. Kuklik P, Zeemering S, Maesen B, Maessen J, Crijns HJ, Verheule S, Ganesan AN, Schotten U. Reconstruction of instantaneous phase of unipolar atrial contact electrogram using a concept of sinusoidal recomposition and Hilbert transform. *IEEE Trans Biomed Eng* 2015;**62**:296–302.
12. Lee P, Calvo CJ, Alfonso-Almazan JM, Quintanilla JG, Chorro FJ, Yan P, Loew LM, Filgueiras-Rama D, Millet J. Low-cost optical mapping systems for panoramic imaging of complex arrhythmias and drug-action in translational heart models. *Sci Rep* 2017;**7**:43217.
13. Herron TJ, Lee P, Jalife J. Optical imaging of voltage and calcium in cardiac cells & tissues. *Circ Res* 2012;**110**:609–623.
14. Zhao J, Hansen BJ, Wang Y, Csepe TA, Sul LV, Tang A, Yuan Y, Li N, Bratasz A, Powell KA, Kilic A, Mohler PJ, Janssen PML, Weiss R, Simonetti OP, Hummel JD, Fedorov VV. Three-dimensional integrated functional, structural, and computational mapping to define the structural "fingerprints" of heart-specific atrial fibrillation drivers in human heart ex vivo. *J Am Heart Assoc* 2017;**6**:e005922.
15. Filgueiras-Rama D. Sympathetic innervation and cardiac arrhythmias. In DP Zipes, J Jalife, WG Stevenson (eds). *Cardiac Electrophysiology: From Cell to Bedside*. 7th ed. Philadelphia, USA: Elsevier; 2017.
16. Li F, Yuan Y. Meta-analysis of the cardioprotective effect of sevoflurane versus propofol during cardiac surgery. *BMC Anesthesiol* 2015;**15**:128.
17. Yan P, Acker CD, Zhou WL, Lee P, Bollensdorff C, Negrean A, Lotti J, Sacconi L, Antic SD, Kohl P, Mansvelder HD, Pavone FS, Loew LM. Palette of fluorinated voltage-sensitive hemicyanine dyes. *Proc Natl Acad Sci USA* 2012;**109**:20443–20448.
18. Matiukas A, Mitrea BG, Qin M, Pertsov AM, Shvedko AG, Warren MD, Zaitsev AV, Wuskell JP, Wei MD, Watras J, Loew LM. Near-infrared voltage-sensitive fluorescent dyes optimized for optical mapping in blood-perfused myocardium. *Heart Rhythm* 2007;**4**:1441–1451.
19. Girouard SD, Laurita KR, Rosenbaum DS. Unique properties of cardiac action potentials recorded with voltage-sensitive dyes. *J Cardiovasc Electrophysiol* 1996;**7**:1024–1038.

20. Hooks DA, LeGrice IJ, Harvey JD, Smaill BH. Intramural multisite recording of transmembrane potential in the heart. *Biophys J* 2001;**81**:2671–2680.
21. Fedorov VV, Lozinsky IT, Sosunov EA, Anyukhovsky EP, Rosen MR, Balke CW, Efimov IR. Application of blebbistatin as an excitation-contraction uncoupler for electrophysiologic study of rat and rabbit hearts. *Heart Rhythm* 2007;**4**:619–626.
22. Brack KE, Narang R, Winter J, Ng GA. The mechanical uncoupler blebbistatin is associated with significant electrophysiological effects in the isolated rabbit heart. *Exp Physiol* 2013;**98**:1009–1027.
23. Knisley SB, Justice RK, Kong W, Johnson PL. Ratiometry of transmembrane voltage-sensitive fluorescent dye emission in hearts. *Am J Physiol Heart Circ Physiol* 2000;**279**: H1421–H1433.
24. Gush RJ, King TA. Discrimination of capillary and arterio-venular blood flow in skin by laser Doppler flowmetry. *Med Biol Eng Comput* 1991;**29**:387–392.
25. Singh-Moon RP, Marboe CC, Hendon CP. Near-infrared spectroscopy integrated catheter for characterization of myocardial tissues: preliminary demonstrations to radiofrequency ablation therapy for atrial fibrillation. *Biomed Opt Express* 2015;**6**: 2494–2511.
26. Tai DC, Caldwell BJ, LeGrice IJ, Hooks DA, Pullan AJ, Smaill BH. Correction of motion artifact in transmembrane voltage-sensitive fluorescent dye emission in hearts. *Am J Physiol Heart Circ Physiol* 2004;**287**:H985–H993.
27. Bishop MJ, Plank G. Simulating photon scattering effects in structurally detailed ventricular models using a Monte Carlo approach. *Front Physiol* 2014;**5**:338.
28. Dillon SM, Kerner TE, Hoffman J, Menz V, Li KS, Michele JJ. A system for in-vivo cardiac optical mapping. *IEEE Eng Med Biol Mag* 1998;**17**:95–108.
29. Lee P, Taghavi F, Yan P, Ewart P, Ashley EA, Loew LM, Kohl P, Bollensdorff C, Woods CE. In situ optical mapping of voltage and calcium in the heart. *PLoS One* 2012;**7**:e42562.
30. Herranz D, Lloret J, Jimenez-Valero S, Rubio-Guivernau JL, Margallo BE. Novel catheter enabling simultaneous radiofrequency ablation and optical coherence reflectometry. *Biomed Opt Express* 2015;**6**:3268–3275.
31. Bourier F, Gianni C, Dare M, Deisenhofer I, Hessling G, Reents T, Mohanty S, Trivedi C, Natale A, Al-Ahmad A. Fiberoptic contact-force sensing electrophysiological catheters: how precise is the technology? *J Cardiovasc Electrophysiol* 2017;**28**:109–114.
32. Schaffer P, Ahammer H, Muller W, Koidl B, Windisch H. Di-4-ANEPPS causes photodynamic damage to isolated cardiomyocytes. *Pflugers Arch* 1994;**426**:548–551.
33. Kanaporis G, Martišienė I, Jurevičius J, Vosyliūtė R, Navalinskas A, Treinys R, Matiukas A, Pertsov AM. Optical mapping at increased illumination intensities. *J Biomed Opt* 2012;**17**:96007–96001.
34. Fedorov VV, Glukhov AV, Chang R, Kostecki G, Aferol H, Hucker WJ, Wuskell JP, Loew LM, Schuessler RB, Moazami N, Efimov IR. Optical mapping of the isolated coronary-perfused human sinus node. *J Am Coll Cardiol* 2010;**56**:1386–1394.
35. Fedorov VV, Ambrosi CM, Kostecki G, Hucker WJ, Glukhov AV, Wuskell JP, Loew LM, Moazami N, Efimov IR. Anatomic localization and autonomic modulation of atrioventricular junctional rhythm in failing human hearts. *Circ Arrhythm Electrophysiol* 2011;**4**:515–525.
36. Martisiene I, Macianskiene R, Treinys R, Navalinskas A, Almanaityte M, Karciauskas D, Kucinskas A, Grigaleviciute R, Zigmantaite V, Benetis R, Jurevicius J. Voltage-sensitive fluorescence of indocyanine green in the heart. *Biophys J* 2016;**110**:723–732.
37. Vidmar D, Krummen DE, Hayase J, Narayan SM, Ho G, Rappel WJ. Spatiotemporal progression of early human ventricular fibrillation. *JACC Clin Electrophysiol* 2017;**3**: 1437–1446.
38. Quintanilla JG, Moreno J, Archondo T, Usandizaga E, Molina-Morúa R, Rodríguez-Bobada C, González P, García-Torrent MJ, Filgueiras-Rama D, Pérez-Castellano N, Macaya C, Pérez-Villacastín J. Increased intraventricular pressures are as harmful as the electrophysiological substrate of heart failure in favoring sustained reentry in the swine heart. *Heart Rhythm* 2015;**12**:2172–2183.
39. Christoph J, Luther S. Marker-free tracking for motion artifact compensation and deformation measurements in optical mapping videos of contracting hearts. *Front Physiol* 2018;**9**:1483.